

Effect of Flow Rate on the Corrosion Behavior of N80 Steel in Simulated Oil Field Environment Containing CO₂ and HAc

Qingwei Niu¹, Zili Li^{1*}, Gan Cui¹, Bingying Wang²

¹ College of Pipeline and Civil Engineering, China university of petroleum (East China), Qingdao, China, 266580

² College of Mechanical and Electronic Engineering, China university of petroleum (East China), Qingdao, China, 266580

*E-mail: zilimenhuzu@163.com

Received: 15 July 2017 / Accepted: 4 September 2017 / Published: 12 October 2017

In most oil and gas fields, CO₂ corrosion has become a significant problem plaguing the development of the oil industry. The usage of Acetic acid (HAc) as a common material in oil extraction increases the complexity of CO₂ corrosion process. Among the many factors affecting the oil casing corrosion, the flow rate plays a decisive role. Therefore, in this work Wuhan Koster CS310 Electrochemical Station was used to measure the dynamic potential polarization curves and perform electrochemical impedance spectroscopy (EIS) at different concentrations of HAc and flow rates. Subsequently, the polarization curves were fitted to obtain the polarization characteristics, and corresponding equivalent circuits were chosen to fit the experimental EIS data. In the end, the corrosion behavior and corrosion mechanism of N80 steel were discussed based on corrosion electrochemical theory. It is concluded that the presence of HAc increases the self-corrosion potential E_{corr} and self-corrosion current density I_{corr} of N80 steel in saturated CO₂ solution, promotes the anodic and cathodic reaction speed, and reduces the thickness and the protective effect of the corrosion product film. Furthermore, it is observed that the flow rate increases the corrosion current density of N80 steel, increases the electric double layer capacitance CPE, reduces the charge transfer resistance R_t , and eventually accelerates the corrosion rate of steel.

Keywords: HAc; CO₂; Flow rate; Corrosion behavior

1. INTRODUCTION

Because of the harsh environment in which oil and gas exploration is conducted, the underground corrosive environment where the pipelines are located is getting worse. In most oil and gas fields, corrosive media and CO₂ content are high, due to which CO₂ corrosion has become

significant issue plaguing the development of the oil industry [1-3]. It was acknowledged that CO₂ corrosion is one of the major issues causing the failure of oil well tubes. Acetic acid (HAc) is the most abundant organic acid in the oil production and transportation which increases the complexity of CO₂ corrosion process. As a result, studying CO₂ corrosion in HAc environments has drawn increasing attention [4-12]. It is generally believed that the local corrosion of carbon steel was promoted due to the decrease of pH in the presence of HAc in the corrosive environment. Zhu et al. [6] studied N80 carbon steel in formation water containing CO₂ and found that HAc enhanced the localized corrosion process. Amri et al. [13-14] studied the effect of HAc on the localized corrosion of carbon steel by an artificial pit and concluded that HAc has a substantial effect on the stage of propagation of localized corrosion. Li et al. [15] studied the crevice corrosion of carbon steel in CO₂-saturated environment and found that corrosion rate increased with the concentration of HAc. However, contrary to the above reports, Nafday and Nescic [16] reported that HAc cannot cause any localized corrosion. Hence, the influence of HAc on CO₂ corrosion is still a controversial subject. Zhang et al. [9] studied the electrochemical corrosion behavior of X65 steel in CO₂-containing environment and found that the presence of HAc could significantly accelerate the reaction rate at the anode and the cathode. Garsany et al. [11] studied the corrosion behavior of X65 steel in 3% NaCl saturated CO₂ environment using voltammetry, and found that HAc promoted the reaction rate at the anode and affected the composition and thickness of the corrosion product film. Crolet et al. [12] considered that HAc could suppress the anodic reaction process. Nescic et al. [17] used the potential polarization curve, EIS, and other methods and had found that the anodic reaction was controlled by charge transfer processes. However, HAc had no effect on the anodic reaction process of carbon steel. Among the many factors affecting the oil casing corrosion such as temperature, pressure, flow rate, corrosion medium and so on, the flow rate played a decisive role. Zhang et al. [18-19] studied the hydrodynamic effects of fluid flow on the flow accelerated corrosion by combining the array electrode technique with computational fluid dynamics (CFD) simulation and demonstrated that the distributions of flow velocity and shear stress affected the corrosion rates.

In this paper, the study of corrosion behavior of oil casing N80 steel under different concentrations of HAc and flow rate has been reported, and its corrosion behavior and corrosion mechanism were also discussed. The results will provide guidance for the comprehensive treatment of CO₂ corrosion in oil field.

2. EXPERIMENTAL

The material under study was oil casing N80 steel, whose chemical composition (wt.%) was 0.42% C, 0.25% Si, 1.50% Mn, 0.012% P, 0.015% S, 0.051% Cr, 0.18% Mo, 0.005% Ni, and Fe as the balance. The epoxy resin was used to encapsulate the working electrode with a size of 10 mm×10 mm. The sample surface was gradually polished to 1200 # using water abrasive paper, and then washed by distilled water, acetone and anhydrous ethanol.

The experimental solution was based on the composition of the oilfield simulated extraction liquid, of which the ion content was shown in Table 1. HAc was added and its concentration in the

solution was 0, 1000 ppm and 5000 ppm, respectively. At the same time, CO₂ was injected into the solution till its level got saturated. All the reagents used in the experiments were of analytical grade.

Table 1. Ion composition of produced liquid in an oil field

Ion composition	K ⁺	Na ⁺	Ca ²⁺	Cl ⁻	SO ₄ ²⁻	Mg ²⁺	HCO ₃ ⁻
Contents (mg/L)	3.13	5912.47	134.67	8862.50	69.16	140.03	1463.82

Wuhan Koster CS310 Electrochemical Station was used to measure the dynamic potential polarization curve and perform the electrochemical impedance spectroscopy (EIS). A three-electrode system was built for conducting the electrochemical tests. A saturated calomel electrode (SCE) was used as the reference, the auxiliary electrode was graphite electrode, and the working electrode is the N80 steel. The scanning rate of the potential polarization curve was 0.5 mV/s, and the scanning range was maintained between ± 300 mV (relative to the open circuit potential). Electrochemical impedance spectroscopy (EIS) was conducted between frequencies 100 kHz and 10 mHz, and the AC excitation signal was a sine wave with an amplitude of ± 5 mV. A temperature of 80 °C was maintained during the experimental process. In order to study the effects of different flow rates on the CO₂ corrosion of N80 steel, DF-101S collector magnetic stirrer was used to adjust the different speed simulations.

3. RESULTS

3.1 Polarization curves

Fig. 1 shows the polarization curves of N80 steel in the simulated environment of oilfield in the presence of saturated CO₂ and different concentrations of HAc. It can be found that the cathode current density is minimized when the effluent is not added with HAc.

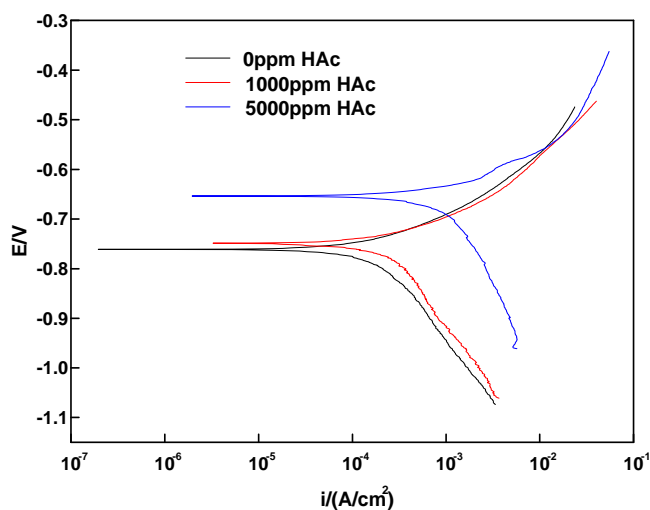


Figure 1. Polarization curves of N80 steel in the simulated environment of oilfield in the presence of saturated CO₂ and different concentrations of HAc.

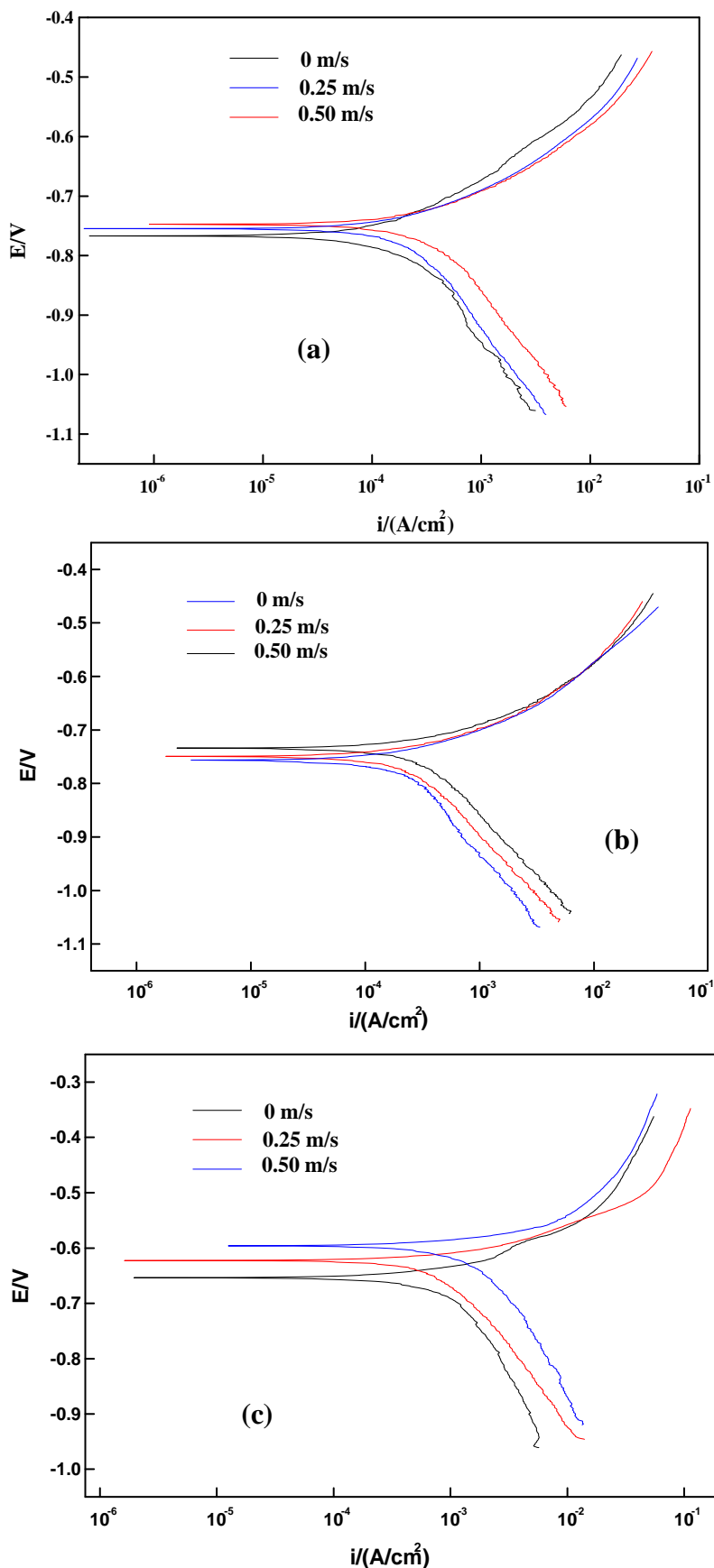


Figure 2. Polarization curves of N80 steels in the simulated environment of oilfield with saturated CO₂ and different flow rates. (a) 0 ppmHAc; (b) 1000 ppmHAc; (c) 5000 ppmHAc

With the increase in the concentration of HAc, the self-corrosion current density I_{corr} and the cathodic current density increase gradually. However, the presence of HAc has little effect on the anodic current density.

Fig. 2 shows the polarization curves of N80 steels in the simulated environment of oilfield in the presence of saturated CO₂, at different flow rates. It can be found that the self-corrosion potential E_{corr} and cathodic polarization current of N80 steel, both increase with the increase of flow rate.

Table 2 present the fitting parameters of polarization curves of N80 steel as obtained for the simulated oilfield environment in the presence of saturated CO₂. Observing the fitting parameters one can see that for N80 steel, the Tafel slope b_c of the cathodic polarization curve is larger than the Tafel slope b_a of the anodic polarization curve, indicating that the cathodic reaction is the main control step for the whole reaction. It also can be concluded that the addition of HAc causes the self-corrosion current density of N80 steel to increase, thereby increasing the corrosion rate. Furthermore, with the increase of flow rate, the corrosion rate also shows an increasing trend.

Table 2. Fitting parameters of polarization curves of N80 steel in simulated oilfield environment with saturated CO₂

HAc concentra- tions/ppm	Flow rate/(m/ s)	E_{corr}/V	$I_{corr}/(A/cm^2)$	$b_a/(mV/decade)$	$b_c/(mV/decade)$	$V_{corr}/(mm/a)$
0	0	-0.7608	8.771×10^{-5}	75.622	-91.303	4.235
	0.25	-0.7516	9.0866×10^{-5}	51.5	-102.29	4.388
	0.50	-0.7519	9.6846×10^{-5}	57.036	-83.34	4.676
1000	0	-0.7590	9.9489×10^{-5}	57.77	-89.189	4.804
	0.25	-0.7480	0.0001056	48.298	-101.05	5.099
	0.50	-0.7443	0.0001117	55.186	-80.056	5.656
5000	0	-0.6526	1.1106×10^{-4}	16.704	-25.641	5.363
	0.25	-0.6246	2.087×10^{-4}	33.255	-89.918	14.077
	0.50	-0.6005	4.6303×10^{-4}	26.313	-68.506	22.358

3.2 Electrochemical impedance spectroscopy (EIS)

Fig. 3 shows the EIS of N80 steel at different HAc concentrations in saturated CO₂ simulated oilfields environment. It can be seen from the figure that when the concentration of HAc is 0 ppm, there is a large capacity resistive arc in the high frequency stage and a small resistance arc at low frequency. The former represents the charge transfer reaction between the corrosion solution and the corrosion product layer, while the latter represents the charge transfer process between layer and metal matrix interface. The corresponding equivalent circuit is shown in Fig. 5 (a). When the concentration of HAc is 1000 ppm, there is still a large capacity of the arc corresponding to the high frequency stage and a small capacity of the arc in the low frequency stage. However, its capacity arc radius is reduced, indicating that the impedance value decreases. The equivalent circuit for this process is also as shown in Fig. 5 (a). When the concentration of HAc is 5000 ppm, there is a large capacity arc in the high

frequency stage, an inductance arc in the intermediate frequency stage, and a small capacity arc in the low frequency stage. These three stages represent the interface charge transfer reaction between the corrosion solution and corrosion product layer, the formation and adsorption process of intermediates, and the dissolution of corrosion products, respectively. The corresponding equivalent circuit is shown in Fig. 5 (b). With the increase of HAc concentration, the radius of the capacitive arc for the high frequency and the low frequency stage decreases gradually.

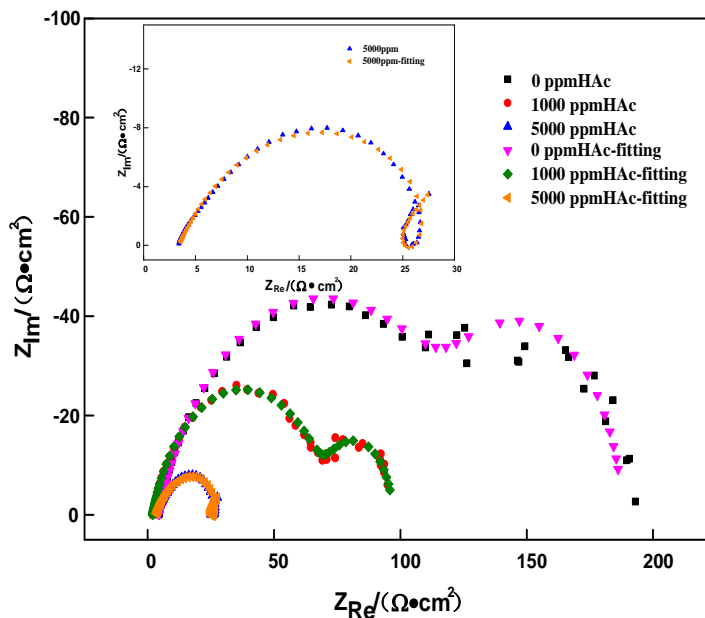
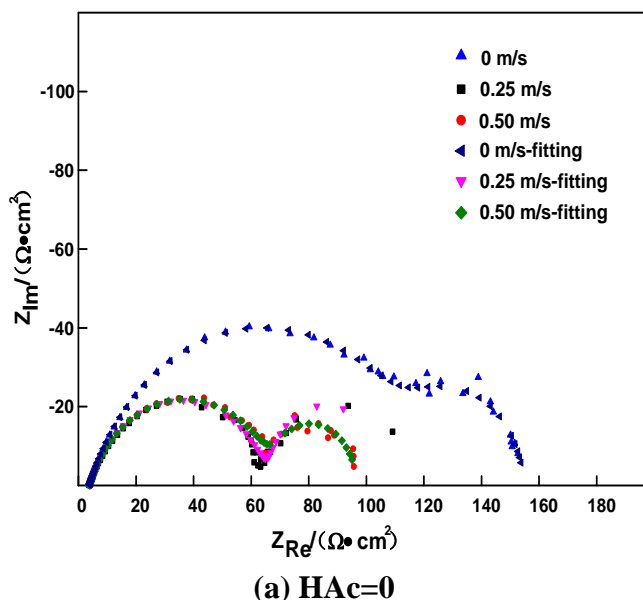
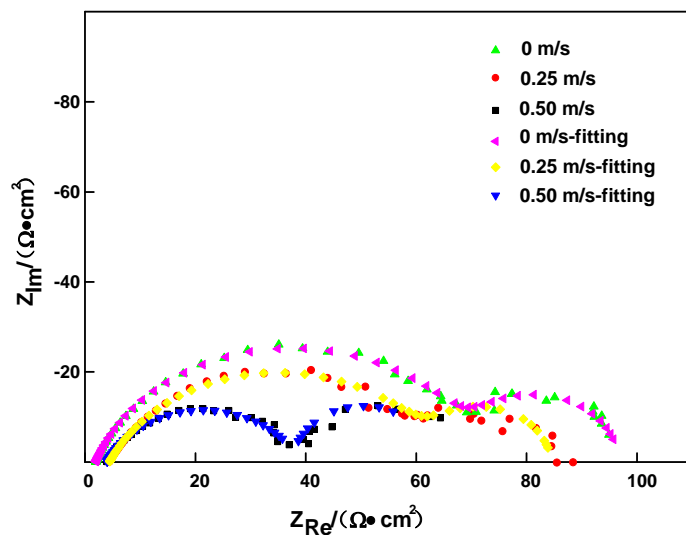


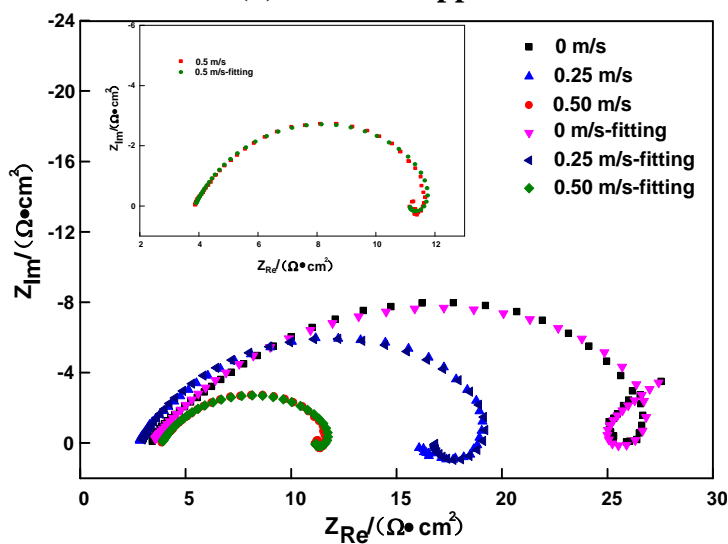
Figure 3. EIS of N80 steel at different HAc concentrations in saturated CO₂ simulated oilfields environment

Fig. 4 shows the EIS of N80 steel at different flow rates in saturated CO₂ simulated oilfield environment. Fig. 4 (a) and (b) depict the EIS corresponding to different flow rates when the HAc concentrations are between 0 and 1000 ppm, respectively.



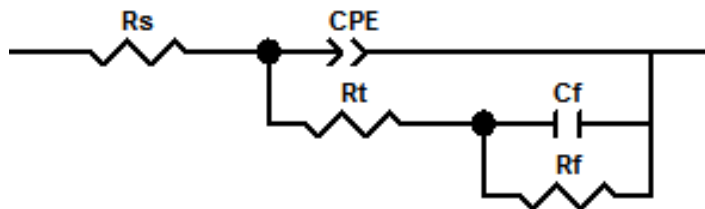


(b) HAC=1000 ppm

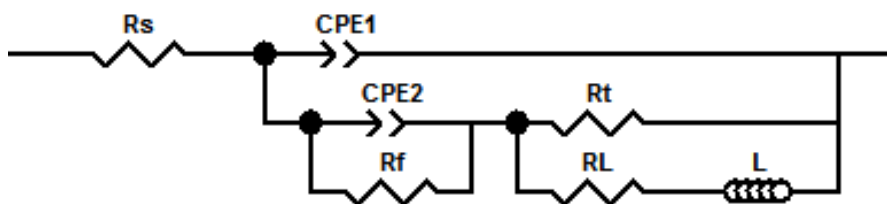


(c) HAC=5000 ppm

Fig. 4. EIS plot of N80 steel at different flow rates in saturated CO₂ simulated oilfield's environment



(a)



(b)

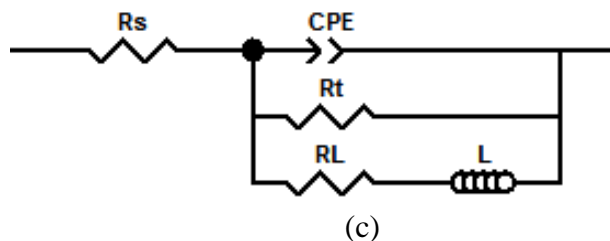


Fig. 5. Equivalent circuits corresponding to EIS plots

At different flow rates, two capacitive arcs exist, and with the increase of the flow rate, the resistive arc radius at high frequency stage and low frequency stage decreases gradually, indicating that the impedance value decreases with the increase of the flow rate. When the concentration of HAC is 5000 ppm, at the flow rate of 0, a large capacity arc exists in the high frequency stage, an inductance arc in intermediate frequency stage, and a small capacity arc in low frequency stage. However, when the flow rates are increased to 0.25 and 0.50 m/s, the resistive arc in the low frequency stage disappears, and only the resistive arc in the high frequency stage and the inductance arc in the low frequency stage continue to exist. Furthermore, with the increase of the flow rate, the capacity arc radius in the high frequency stage decreases. The equivalent circuit depicting this process is shown in Fig. 5 (c).

The EIS data represented in Fig. 3 and Fig. 4 are fitted using the equivalent circuits which are shown in Figure 5. In Fig. 5, R_s depicts the solution resistance, R_t is the charge transfer resistance, CPE_1 (CPE) is the constant phase element of the electric double layer capacitor, C_f is the capacitance of the corrosion product, R_f is the resistance of the corrosion product, CPE_2 is the constant phase element of the surface chemical reaction, R_L is the resistance of the intermediate product formation or dissolution process, and L is the inductance of the intermediate product formation or dissolution process. Table 3 and Table 4 are the fitting parameters for the electrochemical impedance spectroscopy equivalent circuit.

Table 3. Fitting parameters for the electrochemical impedance spectroscopy equivalent circuit of N80 steel (HAc=0 and 1000 ppm)

HAc concentrations/ppm	Flow rate m/s	$R_s/(\Omega \cdot cm^2)$	$CPE/(\Omega^{-1} \cdot cm^{-2} \cdot s^{-n})$	n	$R_t/(\Omega \cdot cm^2)$	$C_f/(F \cdot cm^{-2})$	$R_f/(\Omega \cdot cm^2)$
0	0	3.84	0.00079	0.748	119.7	0.042	31.82
	0.25	3.61	0.00096	0.741	66.30	0.099	26.98
	0.50	3.91	0.0010	0.762	63.35	0.297	39.36
1000	0	3.94	0.00095	0.787	70.94	0.0893	24.05
	0.25	4.44	0.00114	0.734	60.84	0.099	19.30
	0.50	3.96	0.0014	0.742	34.93	0.411	24.2

Table 4. Fitting parameters for the equivalent circuit for the EIS of N80 steel (HAc=5000 ppm)

Flow rate/ (m/s)	$R_s/$ ($\Omega \cdot \text{cm}^2$)	$\text{CPE}_1/$ ($\Omega^{-1} \cdot \text{cm}^{-2} \cdot \text{s}^{-n_1}$)	n_1	$R_f/$ $\Omega \cdot \text{cm}^2$	$\text{CPE}_2/$ ($\Omega^{-1} \cdot \text{cm}^{-2} \cdot \text{s}^{-n_2}$)	n_2	$R_i/$ ($\Omega \cdot \text{cm}^2$)	$R_L/$ ($\Omega \cdot \text{cm}^2$)	$L/$ ($\text{H} \cdot \text{cm}^{-2}$)
0	3.404	0.001	0.64	59.7	0.31	0.528	27.8	83.1	7.1
0.25	3.864	0.002	0.71	—	—	—	18.2	46.57	5.169
0.50	3.869	0.002	0.70	—	—	—	8.703	47.84	4.095

4. DISCUSSION

4.1 Influence of HAc on corrosion behavior of N80 steel

In the saturated CO_2 simulated oilfield effluent environment, the cathodic reactions are described as follows.



The anode reaction is as follows [9]:



Fig. 1 shows the polarization curves at different concentrations of HAc. In the absence of HAc (pH=5.4), the cathodic current density is the lowest, and the cathodic reaction is primarily described by formula (2) and (3). When the HAc is added to the solution, the cathodic reaction that takes place can be represented by formula (1) and (5). According to the polarization, cathodic current density increases, that is, the corrosion rate increases. This is because the addition of HAc reduces the pH of the solution, and promotes the reactions at the cathode. It can be seen from Fig.1 that the addition of HAc has tremendous influence on the cathodic polarization curve, while it has little effect on the anodic polarization curve. These results are similar to those found in a previously reported paper [20] and are because HAc promotes the cathodic reaction and inhibits the anodic reaction process [9].

Fig. 3 shows the EIS plot of N80 steel recorded at different concentrations of HAc in saturated CO_2 simulated oilfield's environment. When the concentration of HAc < 1000 ppm, there are two capacitive arcs in the EIS curves. The capacitive arc in the high frequency stage is representative of the electric double layer capacitance at the interface between corrosion product film and the solution. At low frequencies, there exists a defect in the corrosion product film, and a charge transfer process at the

interface between the corrosion product layer and the metal substrate takes place, resulting in a small capacitive arc, which is consistent with a previously reported work [9, 21-22]. Relative to HAc = 0 ppm, when HAc=1000 ppm, the arc resistance radius is significantly reduced at the low frequency stage. When the HAc=5000 ppm, the high frequency and low frequency phase is still capacitive arc. The high frequency stage represents the charge transfer process in the interface between the corrosion product and the solution. The low frequency represents the formation and dissolution process of the corrosion product i.e. FeCO_3 [22]. However, the existence of the inductance arc in the intermediate frequency stage can be correlated with the formation and adsorption of intermediates, and the corresponding reaction is depicted by formula (6). It can be seen from Table 3 and Table 4 that with the increase in the concentration of HAc, the charge transfer resistance from the equivalent circuit fitting parameters decreases and the electric double layer capacitance increases. According to Eq. (12) [23], the double-layer capacitance CPE increases, resulting in a decrease in the thickness of the corrosion product film L_{ex} . It could be illustrated that the addition of HAc reduces the thickness and increases the defect of the corrosion product film. Thus, the degradation of the matrix is reduced, and the corrosion of the substrate is accelerated, which is consistent with the results of the polarization curve depicted in Fig. 1.

$$L_{ex} = \varepsilon_0 \varepsilon_r / \text{CPE} \quad (12)$$

Where, L_{ex} is the oxide space charge layer thickness, ε_0 is the vacuum permittivity (8.85×10^{-14} F/cm), ε_r is the relative dielectric constant of the corrosion product film of Fe at room temperature.

4.2 Effect of flow rate on corrosion behavior of N80 steel

Fig. 2 shows the polarization curves of N80 steel recorded at different flow rates. It can be seen from the figure that the anodic current density increases with the increase of potential, depicting the anodic dissolution characteristics. It can be seen from Table 2 that the self-corrosion potential E_{corr} and the self-corrosion current density I_{corr} increase with the increase of the flow rate. This is because with the increase of the flow rate, the diffusion rate of the depolarization agents such as H_2CO_3 and H^+ increase. Consequently the rate of cathodic depolarization increases, the consumption of electrons increases, and the negative charge formed on the double layer reduces, as depicted in Eq. (1)~(3). On the other hand, the acceleration of the cathodic reaction accelerates the anodic reaction, resulting in an increase in the corrosion current density [7].

Fig. 4 shows the EIS of N80 steel at different flow rates. Fig. 4 (a) and (b) show the EIS plots recorded at different flow rates at HAc concentrations of 0 and 1000 ppm, respectively. The corresponding equivalent circuit is shown in Fig. 5 (a). There are two kinds of resistive arcs corresponding to different flow rates. With the increase of the flow rate, the radius of the resistive arc at high frequency and low frequency stage decreases gradually, indicating a decrease in the value of the impedance with the increase of the flow rate. When the concentration of HAc is 5000 ppm and the flow rate is 0, there is a large capacity of the arc at the high frequency stage, an inductance arc at the intermediate frequency stage and a small resistance arc at the low frequency stage. The equivalent circuit is shown in Fig. 5 (b). However, when the flow rate is 0.25 and 0.50 m/s, the capacitive arc at

the low frequency stage disappears, and only the resistive arc at the high frequency stage and the inductance arc at the low frequency stage continue to exist. The equivalent circuit is shown in Fig. 5 (c). Due to the role of the flow rate, the as formed corrosion product FeCO_3 is difficult to adhere to the electrode surface, resulting in the disappearance of the resistance arc at the low frequency. It can be seen from Table 3 and Table 4 that with the increase of the flow rate, the value of double-layer capacitance CPE increases and the charge transfer resistance R_t decreases. This is because under the action of the flow rate, a tangential force is generated on the surface of the material, the adhesion of the corrosion product FeCO_3 is hindered, and thus, corrosion process is accelerated [22].

5. CONCLUSIONS

(1) The presence of HAc increases the self-corrosion potential E_{corr} and self-corrosion current density I_{corr} of N80 steel in saturated CO_2 solution, promotes the anodic and cathodic reaction speed, and reduces the thickness and the protective effect of the corrosion product film.

(2) The increase of flow rate enhances the cathodic depolarization. Relative to the static solution, the presence of flow rate increases the corrosion current density of N80 steel, increases the electric double layer capacitance CPE, reduces the charge transfer resistance R_t , and eventually accelerates the rate of corrosion of steel.

References

1. Q. L. He, H. M. Meng, H. Y. Yu, Z. S. Fan, X. D. Wang and D. B. Sun, *J. Chin. Soc. Corros. Prot.*, 23 (2007) 186. (in Chinese)
2. C. F. Chen, M. X. Lu, G. X. Zhao, Z. Q. Bai, M. L. Yan and Y. Q. Yan, *Acta Metall.*, 39 (2003) 94. (in Chinese)
3. W. H. Ma, X. H. Pei, F. Gao and C. L. Gao, *J. Chin. Soc. Corros. Prot.*, 27 (2007) 8. (in Chinese)
4. S. Guo, L. Xu, L. Zhang, W. Chang and M. Lu, *Corros. Sci.*, 110(2016) 123.
5. Q. Y. Liu, L. J. Mao and S. W. Zhou, *Corros. Sci.*, 84(2014) 165.
6. S. D. Zhu, A. Q. Fu, J. Miao, Z. F. Yin and G. S. Zhou, *Corros. Sci.*, 53 (2011) 3156.
7. D. Liu, Z. Y. Chen and X. P. Guo, *Anti-Corros. Method. M.*, 55 (2005) 130.
8. G. A. Zhang and Y. F. Cheng, *Corros. Sci.*, 51 (2009) 1589.
9. G. A. Zhang and Y. F. Cheng, *Corros. Sci.*, 51 (2009) 87.
10. M. H. Nazari and S. R. Allahkaram, *Mater. Des.*, 31 (2010) 4290.
11. Y. Garsany, D. Pletcher, B. Hedges, *J. Electroanal. Chem.*, 538 (2002) 285.
12. J. Crolet, A. Dugstad and N. Thevenot, *Corrosion*, 99 (1999) 25.
13. J. Amri, E. Gulbrandsen, R.P. Nogueira, *Electrochim. Acta*, 54 (2009) 7338.
14. J. Amri, E. Gulbrandsen, R.P. Nogueira, *Corros. Sci.*, 52 (2010) 1728.
15. Y. Z. Li, N. Xu, G. R. Liu, X. P. Guo and G. A. Zhang, *Corros. Sci.*, 112 (2016) 426.
16. O. A. Nafday and S. Nestic, *J. Biochem.*, 51 (2005) 3.
17. S. H. Wang, K. George and S. Nestic, *Corrosion*, Houston: NACE Paper (2004) 04375.
18. G. A. Zhang, L. Zeng, H. L. Huang and X. P. Guo, *Corros. Sci.*, 77 (2013) 334.
19. G. A. Zhang and Y. F. Cheng, *Corros. Sci.*, 52 (2010) 2716.
20. Z. F. Yin, W. Z. Zhao, W. Y. Lai, C. X. Lin and S. D. Zhu, *J. Mater. Eng. Perform.*, 19 (2010) 693.
21. F. F. Eliyan, *J. Appl. Electrochem.*, 42 (2012) 233.

22. Sun Y, George K, Nescic S, *Corrosion*, Houston: NACE Paper (2003) 03327.
23. K. Azumi, *J. Electrochem. Soc.*, 134 (1987) 1352.

© 2017 The Authors. Published by ESG (www.electrochemsci.org). This article is an open access article distributed under the terms and conditions of the Creative Commons Attribution license (<http://creativecommons.org/licenses/by/4.0/>).